RESEARCH ARTICLE

Applying magnetic-responsive nanocatalyst-liquid interface for active molecule manipulation to boost catalysis beyond diffusion limit

Nur Amalina binte Mohamed-Ibrahim[+][a], Siew Kheng Boong[+][a], Zhi Zhong Ang[a], Li Shiuan Ng[a], Jia Ying Charlene Tan[a], Carice Chong[a], Hiang Kwee Lee*[a]

[a] N. A. Mohamed-Ibrahim, S. K. Boong, Z. Z. Ang, L. S. Ng, J. Y. C. Tan, C. Chong, Prof. H. K. Lee
Division of Chemistry and Biological Chemistry, School of Physical and Mathematical Sciences
Nanyang Technological University
21 Nanyang Link, Singapore 637371
E-mail: hiangkwee@ntu.edu.sg Website: www.hiangkweelee.com
[+] These authors contributed equally to this work.

Supporting information for this article is given via a link at the end of the document.

Abstract: Efficient nanocatalysis requires swift delivery of reactants to catalytic sites, but the presence of diffusion-dominated, hydrodynamic boundary layers on all heterogeneous catalysts impedes fast chemical transformation. Here, we achieve efficient nanocatalysis by applying a magnetic-responsive nanocatalyst-liquid interface to create a vortex-like flow that rapidly pulls reactants from bulk solution to the catalyst, beyond the diffusion limit. Consequently, our design attains a > 90 % degradation efficiency in < 5 min with reaction kinetics tunable via the nanocatalyst spin rate. Our spinning nanocatalyst notably exhibits reaction kinetics and molecule transfer rates > 10-fold and 30-fold faster than traditional homogenization methods, respectively. This unique molecule delivery design will complement recent advances in active catalytic nanomaterials to realize ideal nanocatalysis in emerging chemical, energy, and environmental applications.

Introduction

Nanocatalysis utilizes nanometer-sized particles as heterogeneous catalyst to expedite chemical reaction between reactant molecules.[1] This emerging catalytic approach promises efficient chemical transformations by exploiting the large specific area and active catalytic sites on nanomaterials to kinetically drive a chemical reaction along an energy-efficient pathway.[2] Notably, the crux of most nanocatalytic designs (e.g. nanomaterial engineering and surface chemistry modification) is to ensure the rapid delivery of reactants from the bulk solution to catalytic sites for maximal catalyst-reactant interactions.[3] Conventional methods to facilitate heterogeneous catalysis typically utilize fixed catalyst bed to prolong the interaction between catalyst and reaction solution, or employ mechanical stirrer to homogenize chemical species in a bulk solution via forced convection.[4] However, the presence of a hydrodynamic boundary layer on virtually all heterogeneous catalysts creates a formidable barrier to reactant transfer because slow and passive molecular diffusion dominates in this layer.[5] This phenomenon arises from the viscous drag at solid-liquid interface, and cannot be effectively eliminated even with strong turbulence flow within the bulk solution; that is, agitation of the solution can only reduce but does not remove the diffusion layer.[6] Consequently, potential mismatch between slow molecular diffusion and fast intrinsic reactivity impedes overall catalytic efficiency, thereby imposing a performance bottleneck in diverse chemical, energy, and environmental catalysis even when highly active nanocatalysts are used.[7] To achieve efficient and swift chemical transformations, we will clearly need to incorporate a new molecule delivery mechanism into nanocatalyst to actively and sustainably supply reactants to the catalytic sites.

Herein, we achieve efficient nanocatalysis by designing a stimuli-responsive interface formed between a nanocatalyst and the reaction solution to accelerate reactant delivery across the diffusion barrier. Our strategy notably integrates both catalytic and magnetic properties into a nanochain-like ensemble that can spin on-demand in the presence of an external rotating magnetic field. When placed in a reaction solution, the mechanical actuation of the nanocatalyst will interact and drag adjacent liquid layers into a collective circular motion (Figure 1A), thereby creating a vortex-like flow that originates from the nanocatalyst-liquid interface. This unique hydrodynamic phenomenon will enable the nanocatalytic ensemble to actively pull reactants from the bulk solution for efficient catalysis, notably tackling the diffusion barrier that cannot be easily resolved using traditional nanocatalytic approaches.

As a proof-of-concept demonstration, we use Fe_3O_4 nanoparticle as the building blocks of the nanochain-like ensemble due to its well-established magnetic and catalytic properties.[8] Our design can be extended to other catalytic materials by coating them onto magnetic Fe_3O_4 nanoparticles in a core-shell or core-satellite configurations. We use Fenton-based degradation of organic pollutant as a model environmental catalysis due to its importance in water purification. Fenton-based degradation typically involves an initial decomposition of H_2O_2 on Fe_3O_4 catalyst to generate hydroxyl radicals that are subsequently utilized to oxidize organic matter into degradation products.[9] Our catalytic design reaches a > 90 % degradation efficiency in < 5 min with tunable reaction kinetics by controlling the nanocatalyst's spin rate between 0 - 700 rpm. More importantly, our spinning nanocatalyst achieves a reaction kinetics and molecule transfer coefficient that are > 10-fold and 30-fold more superior than traditional bulk homogenization methods, respectively. By manipulating molecule transfer beyond

the diffusion limit, our spinnable nanocatalyst offers a unique perspective to enhance nanocatalysis by facilitating the access of reactants to the catalytic sites. We envisage the parallel advancements in the design of (1) dynamic molecule delivery mechanism and (2) active nanocatalyst materials are crucial to achieve high-performance nanocatalysis with broad applications in chemical synthesis, energy conversion, and environmental remediation.

Results and Discussion

Dynamic manipulation of the interface formed between a nanocatalytic ensemble and the reaction solution plays a central role in the rapid delivery of reactants to catalytic sites for efficient chemical transformations (Figure 1A). To create the dynamic nanocatalyst-liquid interface, we first align bifunctional Fe_3O_4 nanoparticles (diameter, 169±30 nm; Figure S1, S2) into chain-like ensembles using permanent magnets (Figure 1B; Figure S3) and *in situ* coat them with a porous SiO_2 shell via a modified Stöber reaction.[10] Notably, we optimize the Fe_3O_4@SiO_2 nanochains with a thin SiO_2 shell (thickness, ~ 80 nm) and a long chain length of ~ 3.5 µm (Figure 1C, D; Figure S4-6) by varying the amount of NH_3 added and magnetic field strength applied during the coating process, respectively. These structural designs are crucial to facilitate molecule transfer across the porous SiO_2 shell, and to efficiently control the nanocatalyst-liquid interface via an external magnetic field. The catalytic ensemble retains its chain-like structure even after the magnets were removed, emphasizing SiO_2 shell is necessary to hold Fe_3O_4 building blocks in their pre-aligned positions. Further characterization on the catalytic ensemble using surface-sensitive X-ray photoelectron spectroscopy (XPS) affirms the complete encapsulation of Fe_3O_4 nanoparticles within a silica shell, as evident from the emergence of characteristic SiO_2 peaks and disappearance of Fe_3O_4 features (Figure 1E; Figure S7).[8b, 11] As-obtained Fe_3O_4@SiO_2 nanochains can be easily maneuvered via an applied magnetic field (Figure 1F), and remain structurally intact after physical treatment such as ultrasonication (Figure S8). Both the excellent magnetic-responsiveness and mechanical robustness of Fe_3O_4@SiO_2 nanochains are crucial for their subsequent application as a spinnable nanocatalyst.

An important attribute to drive hydrodynamics flow and molecule transfer at nanocatalyst-liquid interface lies in the ability of Fe_3O_4@SiO_2 nanochains to spin within a reaction solution. We thus investigate the spinning dynamics of Fe_3O_4@SiO_2 nanochains in water under an applied rotating magnetic field (Figure 2A). In a typical set-up, an aqueous droplet containing the nanochains is dispensed on a Si wafer and placed on top of a commercial magnetic stirrer. The rotating magnetic field is then activated and the spinning process is recorded using a high-speed camera attached to an optical microscope. The nanochain spin rate can subsequently be determined by tracking its orientation and the time required for it to make one complete revolution. In the presence of an applied rotating field of 100 rpm (Figure 2B), we observe that all the nanochains are spinning along its own vertical axis and take 0.60 s to complete one revolution. This observation denotes an effective spin rate of 100 rpm, which coincides with the applied field. By controlling the rotational rates of the applied magnetic field, we can precisely and linearly program nanochain's spin rates between 100 - 700 rpm (Figure S9). It is noteworthy that spin rates beyond 700 rpm were not examined due to the limitation of our optical microscope to accurately track the spinning process. Nevertheless, the synchronous spinning of nanochain with the applied magnetic fields is clearly demonstrated and can be stably sustained for 30 min (< 3 % deviation; Figure 2C). The nanochains also exhibit excellent reproducibility and responsiveness to an external rotating magnetic field, as evident from the swift alternation of their spin rates between 100 and 700 rpm by regulating the applied rotating magnetic field for ten consecutive cycles (Figure 2D). Such programmable maneuver of nanochain using an external magnetic field is vital for it to effectively interact with the solution for precise control over mass transportation. Hereon, we will name the Fe_3O_4@SiO_2 nanochain as spinnable nanocatalyst (SNC) due to its ability to spin under an applied rotating magnetic field.

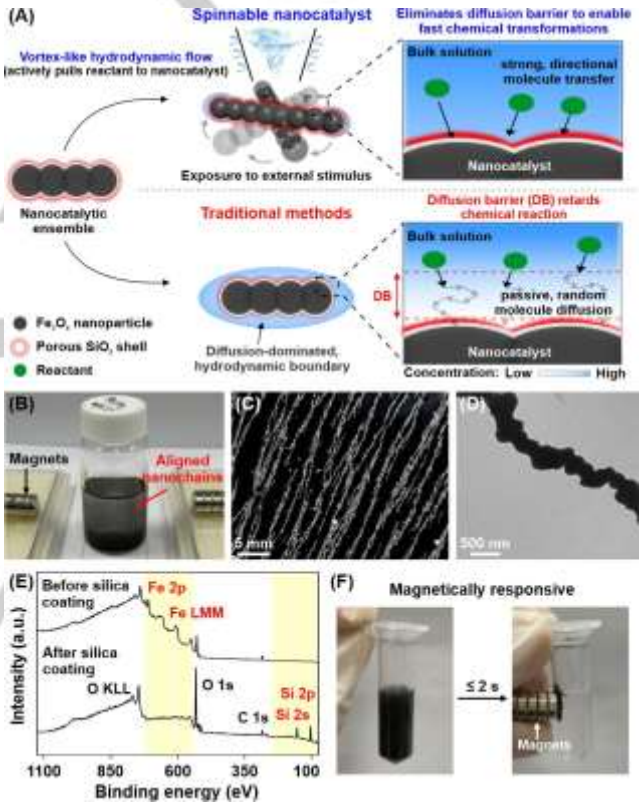

Figure 1. Key concept of spinnable nanocatalyst for enhanced catalysis. (A) Scheme depicting the design and working principles of spinnable nanocatalyst. (B) Experimental set-up to pre-align Fe_3O_4 building blocks into a nanochain-like ensemble for *in situ* SiO_2 coating. (C) Optical image, (D) TEM image, and (E) XPS characterizations of the as-synthesized Fe_3O_4@SiO_2 nanochains. (F) The Fe_3O_4@SiO_2 nanochains are highly responsive to an external magnetic field.

Having affirmed its responsiveness to a rotating magnetic field, we further exploit the nanocatalyst's spinning motion to trigger a hydrodynamic flow for active molecule delivery from bulk solution to the catalyst layer, a key pre-requisite to sustain efficient chemical transformation. To elucidate critical information on the hydrodynamic flow in the presence of static or spinning nanocatalysts, we use an aqueous malachite green droplet (MG; 2 µL) as a dye tracer and track its movement when placed gently on the water surface (~ 2 mL; Figure 2E). Under static condition, the dye tracer experiences an initial fall (Figure S10) due to the

expulsive force created during the dispensing process. However, the dye remains relatively stationary in the middle of the water column (Figure 2F; normalized distance, 0.5) for an extended duration of > 8 s, reaching the bottom catalyst layer only after 20 s. More importantly, we observe that the spinning nanocatalysts (700 rpm) rapidly pulls the dye tracer from the water surface vertically down towards the catalyst layer in < 1 s and spreading the molecules across the entire catalyst layer. The > 25-fold faster mass transfer in spinning nanocatalysts clearly highlights that strong and directed hydrodynamic flow can be triggered to rapidly transport molecules to the catalyst layer, notably across the bulk solution that is > 10^4-fold larger than the nanocatalyst width. We attribute such directional hydrodynamic flow in the bulk solution to the accumulation of multiple tiny vortexes generated by the spinning nanochains at the bottom catalyst layer (details to be discussed later).[12]

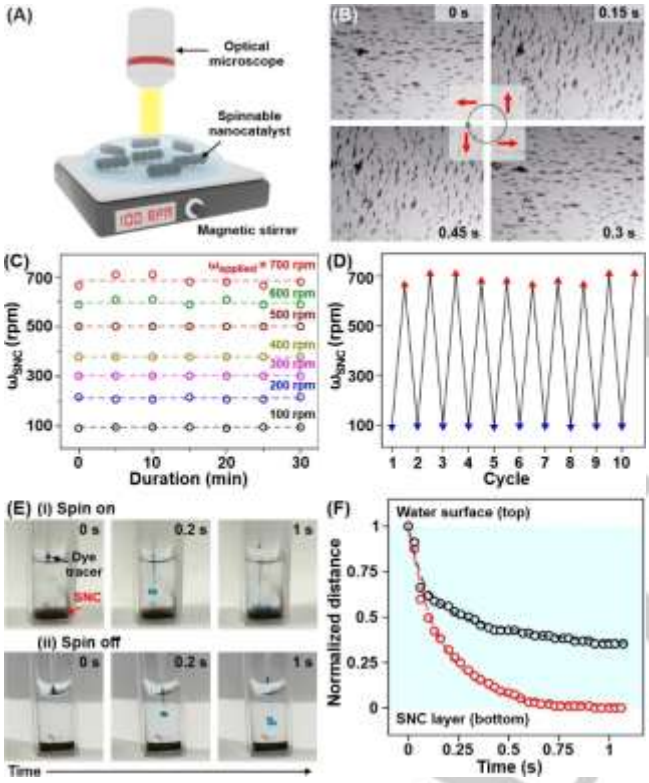

Figure 2. Unravelling spinnable nanocatalyst (SNC) dynamic motion and its influence on bulk hydrodynamic flow. (A) Experimental set-up to investigate the spinning dynamics of Fe_3O_4@SiO_2-based nanocatalyst under an applied rotating magnetic field, as conveyed via a commercial stirrer. (B) Digital images showing the spinning motion of the nanocatalyst. (C) Observed spin rates of the nanocatalyst under an applied rotating magnetic field (100-700 rpm) over a duration of 30 min. (D) Our nanocatalyst's spin rates can be precisely alternated between 100 rpm and 700 rpm by controlling the applied rotating magnetic field. (E) Snapshots on the flow of dye tracer in water when nanocatalyst is (i) spinning at 700 rpm or (ii) is stationary. (F) Quantitative tracking on the flow of dye tracer in (E), starting from the top water surface to the bottom nanocatalyst layer.

Building on the unique hydrodynamic advection enabled by spinning nanocatalyst, we subsequently utilize the dynamic nanocatalyst-liquid interface to swiftly guide molecular reactants across the diffusion barrier to boost catalytic performances. As a proof-of-concept demonstration, we apply spinnable nanocatalyst to achieve efficient environmental catalysis via a cascade Fenton reaction,[8b, 13] whereby hydrogen peroxide (H_2O_2) is first decomposed on Fe_3O_4-based nanocatalyst to generate reactive radical species for subsequent organic pollutant degradation (Figure 3A). We select malachite green as a model because it is a common environmental pollutant that poses severe toxicological/carcinogenic effects to human and the entire ecosystem.[14] A typical catalytic set-up involves the exposure of an aqueous reaction solution containing the nanocatalysts and reactant precursors (equivolume of 1 mM MG and 0.3 %v/v H_2O_2) to an applied magnetic field rotating between 100 – 700 rpm. At pre-defined timings, we extract aliquots of the reaction solution and quantify the non-degraded MG present by correlating its characteristic absorption intensity at 616 nm with an absorbance-concentration calibration curve (Figure 3B, Figure S11).[8a] In the absence of any Fe_3O_4-based nanocatalysts (Figure 3C), no degradation reaction (< 5 %) occurs between the MG and neat H_2O_2 solution over the entire reaction duration of 30 min. This observation allows us to accurately examine the effects of our spinning nanocatalyst on the model reaction by eliminating potential contributions from other origins, such as photodegradation and the reactants' intrinsic reactivity.

To unravel the catalytic and mass manipulation effects of our nanocatalytic design, we first investigate the degradation of organic pollutant (1) under spinning and static conditions, as well as (2) against control catalytic platform involving neat Fe_3O_4 nanoparticles. All nanocatalytic platforms contain the same amount of Fe_3O_4 catalyst (~ 3 mg) for fair comparisons. Time-dependent studies using spinning nanocatalysts (700 rpm) reveal a sharp decrease in MG's absorbance intensity, signifying the rapid access of organic pollutant to the embedded Fe_3O_4 nanocatalyst for rapid degradation (Figure 3B; Figure S12). Spinning nanocatalyst notably achieves an equilibrium degradation efficiency of > 90 % within a short reaction duration of 5 min (C/C_0 = 0.1; C_0 and C denote the MG concentration at 0 min and *t* min, respectively; Figure 3C). In contrast, control experiments involving static spinnable nanocatalyst and Fe_3O_4 nanoparticles exhibit a much slower degradation process, attaining a low degradation efficiency of only 51 % and 36 % at *t* = 30 min, respectively. The slightly better performance of static spinnable nanocatalyst over Fe_3O_4 nanoparticles is due to the larger surface area available when building blocks are held in chains instead of random particle aggregates. By benchmarking the degradation efficiencies at *t* = 5 min (the time for spinning nanocatalyst to reach equilibrium), we deduce that the intrinsic catalytic activity of Fe_3O_4@SiO_2 nanochain accounts for ~ 18 % of degradation efficiency when compared to the absence of catalyst. More importantly, the spinning dynamics of our nanocatalyst accelerates mass transportation and drastically boosts catalytic efficiency by an additional 71 % relative to a static nanocatalyst. We affirm negligible MG adsorption on the spinning nanocatalyst because MG concentration only decreases by < 15 % throughout the entire 30 min (Figure S13). It is also noteworthy that the thickness of silica coating does not affect the nanocatalyst's catalytic performance (< 7 % deviation; Figure S14). Our observations jointly highlight two important findings; (1) pre-alignment of Fe_3O_4 nanoparticles into chain-like ensemble is important for it to spin efficiently under a rotating magnetic field, and (2) the dynamic spinning motion can be harnessed to boost catalytic performance.

We further probe the unique mass transport mechanism at the nanocatalyst-liquid interface to identify the origin of the

enhanced catalysis in spinning nanocatalyst. This information can be gathered by comparing our design with two conventional methods that are commonly used for bulk solution homogenization, namely (1) a commercial micro-stirbar and (2) a bulk vortex shaker. Both bulk homogenization methods are oscillating at an identical rate of 700 rpm and use the same Fe_3O_4@SiO_2 nanochains as catalyst for fair comparisons. Control experiment using commercial micro-stirbar exhibits sluggish reaction with only < 10 % MG degraded within 5 min (Figure 3D), gradually attaining a low equilibrium degradation efficiency of ~ 32 % at *t* = 30 min. Such poor catalytic performance is likely attributed to the drastic decrease in effective catalyst surface area when Fe_3O_4-based nanoparticles are attracted and attached onto the magnetic micro-stirbar (Figure S15).

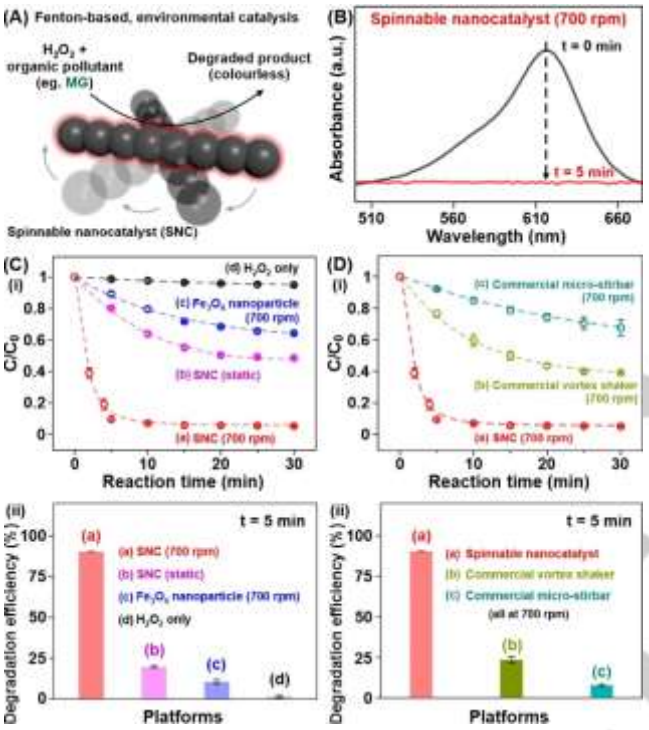

Figure 3. Using spinning nanocatalyst to boost nanocatalysis by overcoming the diffusion barrier in traditional nanocatalytic approaches. (A) Applying Fe_3O_4@SiO_2-based spinnable nanocatalyst to promote Fenton reaction for organic pollutant degradation. (B) Time-dependent absorption spectra of malachite green (MG) in the presence of spinning nanocatalyst. Comparison of spinnable nanocatalyst with (C) other nanocatalytic design and (D) traditional bulk homogenization methods. For (C) and (D), all experiment uses the same amount of Fe_3O_4 building blocks for fair comparisons. (i) Normalized malachite green concentrations (C/C_0) as a function of time during the catalytic reactions. (ii) Comparison of pollutant degradation efficiencies at *t* = 5 min across various experiments.

Next, we also evaluate our spinning nanocatalyst against a commercial vortex shaker that mechanically homogenizes a reaction solution. This bulk mixing method allows a more representative comparison by overcoming the particle aggregation issues that are observed when using a commercial magnetic stirbar. Interestingly, control catalytic set-up using the mechanical vortex shaker also suffers from low degradation efficiencies of ~ 24 % and 61 % at *t* = 5 min and *t* = 30 min (Figure 3D; Figure S13), respectively, despite its well-recognized ability to homogenize a bulk solution. The poorer catalytic efficiency when using a commercial vortex shaker is a concrete evidence that conventional methods cannot efficiently transfer reactants across a hydrodynamic boundary layer, such that the reaction is still diffusion-limited even at identical oscillating rate of 700 rpm.[6, 7b] The superior catalysis in spinning nanocatalyst thus showcases the importance of manipulating nanocatalyst-liquid interface to drive reactants across the diffusion barrier, which is notably distinct from simple mixing and linear actuation reported in other magneto-catalytic systems.[10b, 15]

Thus far, our findings collectively point to the emergence of a unique hydrodynamic flow originating from the dynamic nanocatalyst-liquid interface that is otherwise impossible in bulk homogenization methods (Figure 4A). When exposed to a rotating magnetic field, the magnetic-responsive nanocatalyst spins and drags the solution along with it. Such mechanical rotation will exert a centrifugal force on the hydrodynamic boundary layer, which is a relatively stagnant solvent layer adjacent and strongly interacting with the nanocatalyst surface.[12, 16] The generated centrifugal force notably flings the solution away from the center of the nanocatalyst, allowing the bulk solution to flow towards the nanocatalyst and replace the displaced solution. Consequently, the continuous removal of the diffusion layer by the dynamic nanocatalyst-liquid interactions creates a directional, vortex-like hydrodynamic flow that actively draws reactants from the bulk solution to the catalytic sites, beyond the diffusion limit.[17] In contrast, bulk homogenization methods could only create fluid turbulence to homogenize the bulk solution and aid reactants transfer to the edge of the hydrodynamic boundary layer.[6] However, these traditional approaches cannot effectively eliminate the diffusion barrier which severely hinders reactants transportation to the nanocatalyst. Notably, our findings on a dynamic nanocatalyst-liquid interface is unprecedented, and effectively address the diffusion limit and associated performance bottleneck that exist in virtually all heterogeneous catalysis.[5b, 7, 18]

Besides accelerating mass transfer towards the nanocatalyst, the dynamic manipulation of nanocatalyst-liquid interface doubles as an important handle to modulate reaction kinetics. For instance, systematic increase in nanocatalyst's spin rate from 0 rpm to 700 rpm enhances degradation efficiency from 19 % to > 90 % at *t* = 5 min (Figure 4B; Figure S12), respectively. Our model MG degradation can also be approximated using a pseudo-first-order reaction kinetics with an integrated rate law, $\ln(C/C_0) = -k_{app}t$, where k_{app} and *t* denote the apparent degradation rate constant and reaction time,[8a] respectively. The linear relationships between $\ln(C/C_0)$ and reaction duration observed at all nanocatalyst's spin rate ascertain that MG degradation indeed follows a pseudo-first-order kinetics (Figure 4B(ii)). k_{app} increases by almost 10-fold from 0.05 to 0.45 min^{-1} as we tune nanocatalyst's spin rate from 0 – 700 rpm (Figure 4D), respectively. The significant boost in catalytic performance is due to the stronger centrifugal force and vortex flow created when our nanocatalyst is spinning at a faster rate.[12] In contrast, control experiments using a commercial vortex shaker do not significantly improve MG degradation efficiencies (≤ 61 %) or reaction kinetics (≤ 0.05 min^{-1}), even when oscillation rate increases from 0 rpm to 700 rpm (Figure 4C, D; Figure S13).

More importantly, we also note that nanocatalyst spin rate can be utilized for the precise control over MG molecule transfer rate, as demonstrated by the linear relationship between these two parameters. Our nanocatalytic platform achieves the highest molecule transfer coefficient of 117 μm/s at a spin rate of 700 rpm

(Figure 4E; Supporting Information 1), which is > 30-fold superior over commercial vortex shaker (4 μm/s at 700 rpm; Supporting Information 2) at the same oscillating speed. It is also noteworthy that our design enables 70-fold higher transportation rate than kinesin-based biomolecular motors (1-2 μm/s; known for their rapid mobilization of biomolecules),[19] and possesses fast molecule transfer rate comparable to rotating disc electrode set-up (~ 200 μm/s).[5a, 20] Such rapid molecular transfer is critical to ensure rapid and steady supply of reactants to nanocatalyst for fast chemical transformations. Our magnetic-responsive nanocatalyst is easily recovered in ≤ 2 s using a permanent magnet, and can be reused for at least five repeated catalytic cycles at > 90 % efficiencies while preserving the catalyst's chemical and structural integrities (Figure S16, S17).

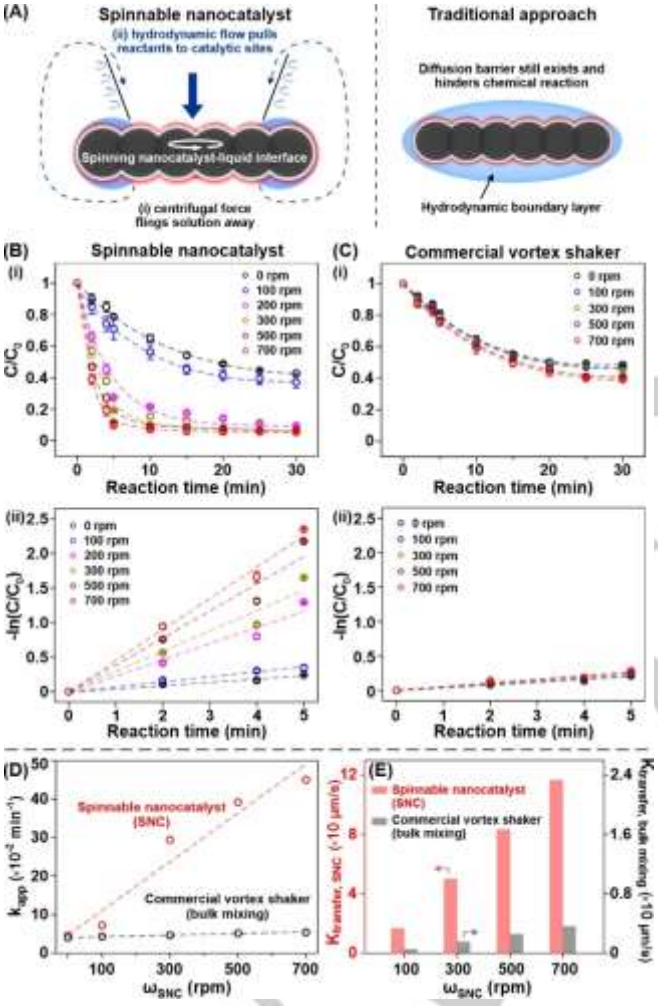

Figure 4. Investigating the reaction kinetics and molecular transfer coefficient attained using spinnable nanocatalyst. (A) Proposed mechanism on the dynamic manipulation of nanocatalyst-liquid interface to direct and accelerate molecule transfer from bulk solution to the catalytic sites. Comparison of the reaction kinetics at various spin/oscillating rates when using (B) spinnable nanocatalyst or (C) commercial vortex shaker. The latter represents a traditional bulk homogenization method. Time-dependent plots of (i) normalized malachite green concentration and (ii) $-\ln(C/C_0)$ at various spin/oscillating rates. Comparison of (D) apparent rate constant (k_{app}) and (E) molecular transfer coefficient ($K_{transfer}$) between spinnable nanocatalyst and commercial vortex shaker at various spin/oscillating rates.

Conclusion

In conclusion, we have achieved efficient nanocatalysis by introducing a spinnable nanocatalyst-liquid interface to accelerate mass transfer across a diffusion-dominated, hydrodynamic boundary layer that is present at all solid-liquid interface. Our strategy focuses on manipulating such dynamic interface using an external stimulus to create a vortex-like flow that actively pulls reactants from bulk solution for rapid reactions. Using an environmental catalysis as a model, our nanocatalyst achieves > 90 % degradation efficiency in less than 5 min with reaction kinetics easily modulated through its spin rate. More importantly, the catalytic ensemble drastically boosts reaction kinetics and molecule transfer coefficient by > 10-fold and 30-fold faster than traditional bulk homogenization methods, respectively, even at identical spin/oscillating rates.

By hastening molecule transfer beyond diffusion limit, our unique design effectively tackles the formidable diffusion barrier and long-standing performance bottleneck in heterogeneous catalysis, which otherwise cannot be easily addressed using conventional nanocatalytic approaches. Our strategy can be easily extended to other nanocatalyst materials by designing hybrid catalytic ensemble using Fe_3O_4 building blocks as magnetic and/or magnetic-heating platforms.[21] Together with the parallel progress in the design of highly-active nanocatalytic materials, our work on integrating an active molecule delivery mechanism into a catalytic ensemble offers an attractive approach to expedite scientific progress towards the design of ideal, efficient nanocatalysts. Achieving efficient nanocatalysis will create enormous opportunities for diverse chemical, energy, and environmental applications, with the aim to address the sustainability crisis faced by mankind.

Experimental Section

Chemicals

Iron(II, III) oxide powder (Fe_3O_4, 95 %), tetraethyl orthosilicate (TEOS, 98 %), ammonium hydroxide solution (28 – 30 %, ACS reagent), and malachite green oxalate salt (dye content, ≥ 90 %) were purchased from Sigma-Aldrich. Hydrogen peroxide (H2O2, 30 %) was from Scharlab. Ethanol (≥ 99.8 %, absolute), acetone (≥ 99.8 %), hexanes (HPLC grade), and 2-propanol (≥ 99.5 %) were purchased from Thermo Fisher Scientific. All chemicals were used without further purification. Milli-Q water (> 18.0 MΩ.cm) was purified with a Sartorius Arium 611 ® UV ultrapure water system.

Synthesis of Fe_3O_4@SiO_2 nanochains

Commercial Fe_3O_4 powders were first washed with ample organic solvents (e.g. ethanol, acetone, hexanes and 2-propanol) to remove any capping agents that could be present on their surfaces. The washed Fe_3O_4 powders were subsequently re-dispersed in 2-propanol at a concentration of ~ 1.5 mg/mL. 2 mL of the Fe_3O_4 suspension was added into a 20 mL reaction vial containing 0.505 mL of TEOS and 4.495 mL of 2-propanol. After which, 1.5 mL of water and 1.5 mL of ammonium hydroxide solution with concentrations ranging from 1 – 10 M (diluted with 2-propanol) were added to the reaction mixture. The reaction solution was quickly homogenized using commercial vortex shaker and immediately placed between two sets of permanent magnets to suspend and align magnetic Fe_3O_4 nanoparticles into

chain-like structures. A modified Stober process was employed and the silica coating process was left to react for 30 min. As-synthesized Fe_3O_4@SiO_2 nanochains were then washed with ample ethanol, and subsequently re-dispersed and stored in ultrapure water. The amount of NH_3 catalyst added as well as the number/distance of permanent magnets used were varied to control the silica coating thickness and the nanochain length, respectively.

Characterizing the spinning dynamics of the nanocatalyst under rotating magnetic field

Approximately 0.5 mL of aqueous suspension containing Fe_3O_4@SiO_2-based spinnable nanocatalyst was dispensed onto a silicon substrate, which in turn was placed on top of a commercial magnetic stirrer. It is noteworthy that the nanochains settled on the commercial stirrer instead of suspending in the solution due to their large particle size and correspondingly stronger magnetic properties. The settling of the nanocatalysts on the Si substrate was crucial to facilitate the facile observation of their spinning behavior via an optical microscope. The spinning of the nanocatalyst was then initiated using an applied magnetic field rotating at 100 – 700 rpm as conveyed by a commercial magnetic stirrer. The spinning process was tracked and recorded using a high-speed camera (~ 35 fps) that was mounted on an optical microscope. The recorded video was then analyzed frame by frame to determine the time required for the nanochain to complete one revolution along its own axis and the corresponding nanocatalyst's spin rate.

Monitoring molecule transfer in bulk solution in presence of spinning nanocatalyst

As-synthesized nanocatalysts were added into 2 mL water in a transparent cuvette that was placed atop of a commercial magnetic stirrer. A rotating magnetic field (700 rpm) was then applied. A 2 µL aqueous malachite green solution (10^{-2} M) was gently dispensed on the water surface. The malachite green solution served as a dye tracer and the hydrodynamic flow in bulk solution was monitored using an optical camera.

Application of spinnable nanocatalysts for Fenton-based oxidative degradation of organic pollutant

A calibration curve relating absorbance intensity and concentration of malachite green was first established. This calibration curve was used for subsequent quantification of malachite green molecules that were left unreacted in the aqueous solution. Briefly, aqueous malachite green (10^{-2} M) solution was first prepared and later serial diluted into various concentrations between 10^{-5} and 10^{-4} M. These malachite green solutions were then measured and quantified using UV-vis spectroscopy.

For the Fenton-based catalysis, all reaction set-ups notably used the same effective mass of Fe_3O_4 (~ 3 mg) to ensure fair comparisons among various catalytic platforms. In a typical set-up, the nanocatalysts were separated from 2-propanol using a permanent magnet and later transferred into a 2 mL centrifuge tube containing 0.5 mL of aqueous malachite green solution (1 mM). 0.5 mL of aqueous H_2O_2 solution (0.3 % v/v) was then added and the reaction vessel was immediately placed on top of a commercial magnetic stirrer with rotational rate controlled between 0 and 700 rpm. A 100 µL aliquot of the reaction solution was extracted at pre-defined intervals of 5 min for a total reaction duration of 30 min. All aliquots collected were placed near a permanent magnet to remove Fe_3O_4-based nanocatalysts, and subsequently transferred to a cuvette for malachite green quantification using UV-visible spectroscopy. Control experiments involving neat Fe_3O_4 nanoparticles and in the absence Fe_3O_4 nanoparticles were also conducted to identify the contributions of catalytic and mass transport properties to the overall degradation efficiency observed in spinning nanocatalyst.

Comparison between spinnable nanocatalyst and traditional bulk homogenization methods

Control experiments involving two conventional bulk homogenization methods were performed to highlight the importance of dynamic nanocatalyst-liquid interface to accelerate mass transportation across traditional diffusion barrier. The two conventional bulk homogenization methods were based on (i) a commercial micro-stirbar and (ii) a bulk vortex shaker. Note that all the experiments used Fe_3O_4@SiO_2 nanochains as catalyst and contained ~ 3 mg of Fe_3O_4. For method (i), Fe_3O_4@SiO_2 nanochains were first added into a 2 mL centrifuge tube containing 0.5 mL of aqueous malachite green solution (1 mM) and a commercial micro-stirbar (5 mm × 2 mm). 0.5 mL of aqueous H_2O_2 solution (0.3 % v/v) was then added and the reaction vessel was immediately placed on top of a commercial magnetic stirrer (700 rpm). A 100 µL aliquot of the reaction solution was extracted at pre-defined intervals of 5 min for a total reaction duration of 30 min. All aliquots collected were placed near a permanent magnet to remove Fe_3O_4@SiO_2 nanochain catalysts, and subsequently quantified using UV-visible spectroscopy.

For method (ii), the oscillation speed of the vortex shaker was first determined using a high-speed optical camera operating at 240 fps. The Fe_3O_4@SiO_2 nanochains was added into a 2 mL centrifuge tube containing 0.5 mL of aqueous malachite green solution (1 mM). 0.5 mL of aqueous H_2O_2 solution (0.3 % v/v) was then added and the reaction vessel was immediately taped upright onto the commercial vortex shaker using an adhesive tape. The vortex shaker was set at an oscillation rate between 0 and 700 rpm, similar to the nanocatalyst's spin rate. A 100 µL aliquot of the reaction solution was extracted at pre-defined intervals of 5 min for a total reaction duration of 30 min. All aliquots collected were placed near a permanent magnet to remove Fe_3O_4@SiO_2 nanochain catalysts, and subsequently quantified using UV-visible spectroscopy.

Reusability of spinnable nanocatalysts

Spinnable nanocatalysts were recovered from a reaction solution within 2 s using a permanent magnet. The nanocatalysts were washed with ample 2-propanol and subsequently re-used repeatedly for multiple catalytic cycles.

Characterization

Transmission electron microscopy (TEM) images were captured on a JEM-1400 (JEOL) operated at 100 kV. Scanning electron microscopy (SEM) imaging was performed with JEOL-JSM-7600F microscope at 5 kV. XPS spectra were measured using a Phoibos 100 spectrometer with a monochromatic Mg X-ray radiation source. Optical microscopy images were captured using a Nikon Eclipse Ci Upright Microscope equipped with a 2.3 megapixel CMOS camera with a frame rate up to 40 fps. UV-vis spectroscopic measurements were conducted using an AvaSpec-

ULS2048CL-EVO-UA-50 equipped with a deuterium-halogen light source (AvaLight-DH-S). A LLG-UNISTIRRER was used as a commercial magnetic stirrer to convey an external magnetic field rotating at 100 – 700 rpm.

Acknowledgements

H.K.L. thanks the funding supports from Singapore Ministry of Education (AcRF Tier 1 RS13/20 and RG4/21), Agency of Science, Technology and Research, Singapore (A*STAR; AME YIRG A2084c0158), and Nanyang Technological University start-up grants.

Keywords: nanocatayst • dynamic interface • diffusion limit • magnetic-responsive • molecule manipulation

[1] D. Astruc, *Chem. Rev.* **2020**, *120*, 461-463.

[2] a) M. Li, K. Duanmu, C. Wan, T. Cheng, L. Zhang, S. Dai, W. Chen, Z. Zhao, P. Li, H. Fei, Y. Zhu, R. Yu, J. Luo, K. Zang, Z. Lin, M. Ding, J. Huang, H. Sun, J. Guo, X. Pan, W. A. Goddard, P. Sautet, Y. Huang, X. Duan, *Nat. Catal.* **2019**, *2*, 495-503; b) C. H. Wu, C. Liu, D. Su, H. L. Xin, H.-T. Fang, B. Eren, S. Zhang, C. B. Murray, M. B. Salmeron, *Nat. Catal.* **2019**, *2*, 78-85; c) C. Xia, Y. Xia, P. Zhu, L. Fan, H. Wang, *Science* **2019**, *366*, 226-231.

[3] a) B. Dong, Y. Pei, F. Zhao, T. W. Goh, Z. Qi, C. Xiao, K. Chen, W. Huang, N. Fang, *Nat. Catal.* **2018**, *1*, 135-140; b) J. Knudsen, T. Gallo, V. Boix, M. D. Strømsheim, G. D'Acunto, C. Goodwin, H. Wallander, S. Zhu, M. Soldemo, P. Lömker, F. Cavalca, M. Scardamaglia, D. Degerman, A. Nilsson, P. Amann, A. Shavorskiy, J. Schnadt, *Nat. Commun.* **2021**, *12*, 6117; c) S. Mitchell, R. Qin, N. Zheng, J. Pérez-Ramírez, *Nature Nanotechnology* **2021**, *16*, 129-139; d) L. Negahdar, C. M. A. Parlett, M. A. Isaacs, A. M. Beale, K. Wilson, A. F. Lee, *Catal. Sci. Technol.* **2020**, *10*, 5362-5385.

[4] a) E. Gross, J. H.-C. Liu, F. D. Toste, G. A. Somorjai, *Nat. Chem.* **2012**, *4*, 947-952; b) X. Du, Y. Huang, X. Pan, B. Han, Y. Su, Q. Jiang, M. Li, H. Tang, G. Li, B. Qiao, *Nat. Commun.* **2020**, *11*, 5811.

[5] L. Burwell, M. Boudart; D. Jaćimovski, R. Garić-Grulović, N. Vučetić, R. Pjanović, N. Bošković-Vragolović, *Powder Technol.* **2016**, *303*, 68-75.

[6] W. Rösing, T. Schildhauer, J. König, C. Cierpka, *Microfluid. Nanofluid.* **2019**, *23*, 110.

[7] a) Y. Lanoiselée, N. Moutal, D. S. Grebenkov, *Nat. Commun.* **2018**, *9*, 4398; b) S. Sarkar, *Phys. Rev. X* **2020**, *10*, 041032.

[8] a) X. Han, H. K. Lee, Y. H. Lee, X. Y. Ling, *J. Phys. Chem. Lett.* **2017**, *8*, 243-249; b) Y. Yin, Y. Ren, J. Lu, W. Zhang, C. Shan, M. Hua, L. Lv, B. Pan, *Appl. Catal., B* **2021**, *286*, 119943.

[9] N. Thomas, D. D. Dionysiou, S. C. Pillai, *J. Hazard. Mater.* **2021**, *404*, 124082.

[10] a) X. Li, H. K. Lee, I. Y. Phang, C. K. Lee, X. Y. Ling, *Anal. Chem.* **2014**, *86*, 10437-10444; b) W. H. Chong, L. K. Chin, R. L. S. Tan, H. Wang, A. Q. Liu, H. Chen, *Angew. Chem. Int. Ed.* **2013**, *52*, 8570-8573.

[11] A. Dane, U. K. Demirok, A. Aydinli, S. Suzer, *J. Phys. Chem. B* **2006**, *110*, 1137-1140.

[12] W. H. Chong, Y. Huang, T. N. Wong, K. T. Ooi, G.-P. Zhu, *Adv. Mater. Technol.* **2018**, *3*, 1700312.

[13] S. Han, H. Yu, T. Yang, S. Wang, X. Wang, *Sci. Rep.* **2017**, *7*, 6070.

[14] a) N. P. Raval, P. U. Shah, N. K. Shah, *Appl. Water Sci.* **2017**, *7*, 3407-3445; b) S. Srivastava, R. Sinha, D. Roy, *Aquat. Toxicol.* **2004**, *66*, 319-329.

[15] a) S. Yang, C. Cao, Y. Sun, P. Huang, F. Wei, W. Song, *Angew. Chem. Int. Ed.* **2015**, *54*, 2661-2664; b) J. Zhou, C. Wang, P. Wang, P. B. Messersmith, H. Duan, *Chem. Mater.* **2015**, *27*, 3071-3076.

[16] a) G. Halász, B. Gyüre, I. M. Jánosi, K. G. Szabó, T. Tél, *Am. J. Phys.* **2007**, *75*, 1092-1098; b) S. C. Shadden, K. Katija, M. Rosenfeld, J. E. Marsden, J. O. Dabiri, *J. Fluid Mech.* **2007**, *593*, 315-331.

[17] J. Nikolic, E. Expósito, J. Iniesta, J. González-Garcia, V. Montiel, *J. Chem. Educ.* **2000**, *77*, 1191.

[18] G. Nagayama, T. Matsumoto, K. Fukushima, T. Tsuruta, *Sci. Rep.* **2017**, *7*, 43125.

[19] *Physics Today* **2002**, *55*, 63-64.

[20] I. Dumitrescu, R. M. Crooks, *Proc. Natl. Acad. Sci. U. S. A.* **2012**, *109*, 11493-11497.

[21] a) S. Gyergyek, A. Kocjan, A. Bjelić, M. Grilc, B. Likozar, D. Makovec, *Materials Research Letters* **2018**, *6*, 426-431; b) S. Gyergyek, A. Kocjan, M. Grilc, B. Likozar, B. Hočevar, D. Makovec, *Green Chemistry* **2020**, *22*, 5978-5983; c) S. Gyergyek, D. Lisjak, M. Beković, M. Grilc, B. Likozar, M. Nečemer, D. Makovec, *Nanomaterials* **2020**, *10*, 1142.

Entry for the Table of Contents

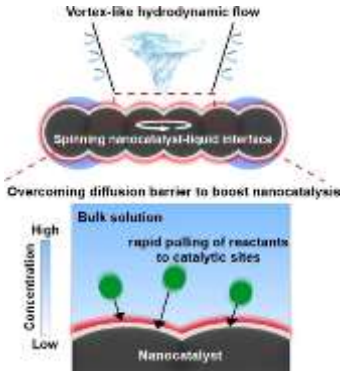

Dynamic manipulation of a spinning nanocatalyst-liquid interface accelerates reactants delivery to catalytic sites via a vortex-like, hydrodynamic flow that originates from the nanocatalytic ensemble. Our design consequently achieves efficient nanocatalysis by enabling fast and steady chemical transformations, notably overcoming the formidable diffusion barrier that occurs at the solid-liquid interface of most heterogeneous (nano)catalysts.